Monthly Notices of the ROYAL ASTRONOMICAL SOCIETY

MNRAS **509,** 2674–2688 (2022) https://doi.org/10.1093/mnras/stab3151
Advance Access publication 2021 October 30

White dwarfs identified in LAMOST Data Release 5

Jincheng Guo,[1,2,3,4]★† Jingkun Zhao,[5,6] Huawei Zhang,[3,4] Jiajun Zhang,[5,6] Yu Bai,[5] Nikolay Walters ,[1] Yong Yang[5,6] and Jifeng Liu[5,6]

[1]*Department of Physics and Astronomy, University College London, London WC1E 6BT, UK*
[2]*Beijing Planetarium, Xizhimenwai Road, Beijing 100044, China*
[3]*Department of Astronomy, Peking University, Beijing 100871, China*
[4]*Kavli Institute for Astronomy and Astrophysics, Peking University, Beijing 100871, China*
[5]*Key Laboratory of Optical Astronomy, National Astronomical Observatories, Chinese Academy of Sciences, Beijing 100012, China*
[6]*University of Chinese Academy of Sciences, Beijing 100049, China*

Accepted 2021 October 27. Received 2021 October 27; in original form 2021 March 16

ABSTRACT

In this paper, we report white dwarfs (WD) identified in the 5th Data Release of the *Large Area Multi-Object fibre Spectroscopic Telescope* (*LAMOST*), including spectral types of DA, DB, DC, DZ, and so on. There are 2625 DA spectra of 2281 DA stars, 182 DB spectra of 166 DB stars, 62 DC spectra of 58 DC stars, 36 DZ spectra of 33 DZ stars, and many other types identified, in addition to our previous paper (Data Release 2). Amongst those sources, 393 DA stars and 46 DB stars are new identifications after cross-matching with the literature. In order to select DA candidates, we use the classification result from the LAMOST pipeline, colour-colour cut method and a random forest (RF) machine learning method. For DBs, since there is no template for DB in the pipeline model, a RF machine learning method is chosen to select candidates. All the WD candidates have been visually checked individually. The parameters of effective temperature, surface gravity, mass, and cooling age have been estimated for relatively high signal-to-noise ratio DAs and DBs. The peaks of the DA and DB mass distributions are found to be around 0.62 and 0.65 $M_{\odot}$, respectively. Finally, the data and method we used to select WD candidates for the second phase of LAMOST survey are also addressed in this paper.

Key words: astronomical data bases: surveys-catalogues – stars: fundamental parameters – stars: white dwarfs.

1 INTRODUCTION

The great majority of main-sequence stars are in the mass range of 0.07–10 $M_{\odot}$, which is also the mass range of white dwarf (WD) progenitors (Doherty et al. 2015). According to the literature (Fontaine, Brassard & Bergeron 2001; Heger et al. 2003), up to 97 per cent of all stars in our Galaxy will eventually evolve to WDs. Based on spectroscopic features, WDs mainly consist of DAs and DBs. They are the most explored types of single WDs, one reason is that they account for 90 per cent of WDs. The specific number of this fraction recently was found vary with the effective temperature (Rolland, Bergeron & Fontaine 2018; Cunningham et al. 2020), based on *Gaia* spectroscopic sample, after significant fraction of cool WDs were discovered (Gentile Fusillo et al. 2019). Another reason is that they are objects of great importance, providing crucial information in various fields. For instance, the simple cooling mechanism of WDs makes it easier to obtain relatively accurate ages. Therefore, for research on the age of Galactic stellar halo (Guo, Liu & Liu 2016; Kilic et al. 2019; Guo et al. 2019), WDs are important age estimation tools after their physics are well-understood. By studying mass distribution (Kepler et al. 2007; Holberg et al. 2016; Hollands et al. 2018) and luminosity functions (Harris et al. 2006; Munn et al. 2017; Lam et al. 2019) of WDs, multiple astrophysical processes of scientific importance can be learnd, in particular, the initial mass function and binary interactions. Meanwhile, WDs can serve as accurate records of star formation and reveal the evolution history of the Milky Way (Krzesinski et al. 2009; Rowell 2013). Additionally, for stars that will eventually evolve to WDs, studies of their initial-final mass relation depend on both single WDs in clusters (Catalán et al. 2008a; Kalirai et al. 2008, 2009) and WDs in binaries (Catalán et al. 2008b; Zhao et al. 2012a), These researchs will help provide important information on the evolution of our Galaxy (Kilic et al. 2017).

The goal to establish a large WD database has been pursued for more than three decades. McCook & Sion (1987) spectroscopically identified 1279 WDs that has been updated to 2249 entries by McCook & Sion (1999). The total number of WDs has increased greatly, with the development of large surveys, e.g. Palomar-Green (Green, Schmidt & Liebert 1986) and Sloan Digital Sky Survey (York et al. 2000, SDSS) particularly (Kleinman et al. 2004; Eisenstein et al. 2006). By using the data release (DR) 7 (Abazajian et al. 2009), Kleinman et al. (2013) spectroscopically identified about 20 000 WDs. Recently, Kepler et al. (2015) made ∼ 9000 new identifications of WDs from SDSS DR10 (Ahn et al. 2014). More recently, around 6000 and 20 000 WDs were identified from SDSS DR12 and DR14, respectively (Kepler et al. 2016, 2019).

★ E-mail: andrewbooksatnaoc@gmail.com
† LAMOST fellow.

The *Large Area Multi-Object fibre Spectroscopic Telescope* (*LAMOST*) pilot survey started in 2012, and the first phase was completed 5 yr later. After a transition from 2017 September to 2018 June, the survey began its second phase. There has been a medium resolution (resolving power $R \sim 7500$) spectroscopy carried out during bright nights in the second phase, together with lower resolution observations during dark nights ($R \sim 1800$). In the 5 yr of the first phase, several studies on LAMOST WDs have been conducted. Zhao et al. (2013) identified 70 DAs from the LAMOST pilot survey. Zhang et al. (2013) presented a catalogue of 230 DAs by fitting Sersic profiles to Balmer lines of spectra. Combining the spectral type results from LAMOST pipeline, the Balmer line equivalent width measurements, and the colour-colour cut method, Guo et al. (2015b) identified 1056 DAs, 34 DBs, 276 white dwarf main sequence (WDMS) binaries and other spectral types of WDs in LAMOST DR2. Gentile Fusillo et al. (2015) also reported the discovery of 253 new WDs in LAMOST DR3. By exploiting a well characterized magnitude limited DA star sample selected from LAMOST Galactic anticentre, space density, formation rate, luminosity, and mass functions of DA WDs were studied (Rebassa-Mansergas et al. 2015). Recently, a catalogue of 876 WDMS binaries identified in LAMOST DR5 are presented by Ren et al. (2018).

Apart from spectroscopic surveys, the studies of WDs have opened a new window since the *Gaia* data released (Gaia Collaboration 2016). Based on *Gaia* data, local complete WD samples have been built separately for 20 pc (Hollands et al. 2018) and 40 pc (Tremblay et al. 2020). There are other much larger but not volume complete WD sample discovered in *Gaia* DR2 (Gaia Collaboration 2018a). Jiménez-Esteban et al. (2018) presented a catalogue of 73 221 WD candidates extracted from DR2. More recently, more than 260 000 high-confidence WD candidates were discovered in DR2, as well (Gentile Fusillo et al. 2019). Evidence for merged WDs has also been revealed (Kilic et al. 2018). By adopting accurate positions, proper motions, and parallaxes, detailed studies on WD kinematics have been conducted by several research groups (Bovy 2017; Gaia Collaboration 2018b; Rowell & Kilic 2019; Torres et al. 2019).

In this work, we present a catalogue of WDs discovered in LAMOST DR5,[1] as well as their physical parameter estimation. In Section 2, we present the selection methods of DAs and DBs. The estimation of the parameters for DAs and DBs (effective temperature, surface gravity, mass, and cooling age) is described in Section 3. We discuss our WD target selection for the second phase of LAMOST in Section 4. Finally, we present our summary in Section 5.

2 CANDIDATES SELECTION

2.1 LAMOST observation

LAMOST is a 4-m reflecting Schmidt telescope, equipped with a multiobject spectrograph that has a 20 deg^2 field of view and 4000 fibres. The LAMOST project began its 1-yr pilot study in 2012, followed by a 5-yr first phase survey. There is only low resolution spectroscopy in the first phase. The spectral resolving power is $R \sim 1800$, covering a wavelength range 3800–9000 Å. With typical exposure times of 1.5 h, the limiting magnitude can reach 20.5 mag (Cui et al. 2012). The first phase survey is composed of two major parts (Zhao et al. 2012b). The first part is the LAMOST Experiment for Galactic Understanding and Exploration (LEGUE) survey, focused on understanding the structure and evolution of the Milky Way (Deng et al. 2012). The second part is the LAMOST Extra-Galactic Survey of galaxies, whose purpose is to study the large-scale structure of the universe. The LEGUE survey consists of three smaller surveys, where each is selected for distinct purposes (Carlin et al. 2012; Chen et al. 2012; Yuan et al. 2015). The targets are mainly chosen from the Galactic disc, spheroid, and anticentre. Although LAMOST is a spectroscopic survey only, there are also photometric data provided by different astronomers from various photometric catalogues, e.g. Xuyi Schmidt Telescope Photometric Survey of the Galactic Anticentre (XSTPS-GAC; Guo et al. 2018), 2MASS, SDSS, Kepler, NVSS, etc. More than 50 per cent of the input catalogue entries at least have *g*, *r*, and *i* magnitudes, mainly from XSTPS-GAC and SDSS. In LAMOST DR5, there are almost 10 million spectra (details in Table 1). Whilst the second phase of LAMOST is ongoing, this work is based on the completed first phase of LAMOST, in particular DR 3, 4, and 5.

2.2 DA selection

The raw spectral data are processed with the LAMOST 2D pipeline (Luo et al. 2015). The standard procedures of dark current subtraction, bias subtraction, cosmic ray removal, 1D spectral extraction, and sub-exposures combination are performed in the process of 2D pipeline. Next, the 1D pipeline is used to perform spectral classification, then calculate the radial velocity for each spectrum. Spectral classification adopted by 1D pipeline is done by template matching. The most important part is to construct a spectral classification template library. The early version of this library for LAMOST is built firstly by excluding outliers using local outlier probabilities, then principal component analysis was used to reconstruct spectra. More description can be found in Wei et al. (2014). The updated version of this library is constructed through clustering algorithm (Kong & Luo 2019). The pipeline classification determines object class (STAR, QSO, GALAXY, and UNKNOWN), and subclass, e.g. (B2, G6, and WD). With better pipeline development and more information, there are more correctly classified spectra in DR5. We successfully identify numerous false positives from our previous catalogue, mostly spectra with low signal-to-noise (S/N) ratio, which we marked ':' for uncertain about the classification (presented in Table 5).

Machine learning has drawn increasing attention in astronomy, where spectral classification is an important potential application (Jiang et al. 2013; Liu et al. 2014; Li et al. 2018). Thus, we applied machine learning algorithm to select DA candidates in this work, as another independent method besides adopting pipeline subclass. There are various types of machine learning algorithms, e.g. support vector machine, Bayesian networks, and decision tree learning. Based on our previous experience performing spectral classification (Bai, Liu & Wang 2018; Bai et al. 2019), we choose an algorithm called random forest (RF Breiman 2001). It performs better than other algorithms, in terms of time cost and accuracy.

The RF algorithm operates by constructing a multitude of decision trees at training and outputting the class that is the mode of the classification of the individual trees (Breiman 2001). Random decision forests correct for decision trees's habit of overfitting to their training set. The RF algorithm implementation used in this work is a supervised algorithm, and adopts 100 trees (estimators). All flux values of a spectrum are used as parameters. The largest weight is given to parameters in the Balmer-line wings. For each spectrum, a probability value will be produced by the RF algorithm. Then a simple binary classification is used. If the probability of being a DA star is greater than 50 per cent, this object will be classified

[1] Spectra available at http://dr5.lamost.org/

Table 1. Updated spectral statistic of each data release for first phase. Note: STAR, GALAXY, QSO, and UNKNOWN are class assigned by LAMOST pipeline. Numbers may change as spectral reduction and classification pipelines update.

Survey	Date	Star	Galaxy	QSO	Unknown	Total
Pilot	2011-10-24 2012-06-17	837 056	8045	1 227	118 060	964 388
DR1	2012-09-28 2013-06-03	1 536 045	12 734	6 035	127 198	1 682 012
DR2	2013-09-10 2014-06-03	1 504 329	30 432	6 382	91 399	1 632 542
DR3	2014-09-10 2015-05-30	1 516 147	26 288	8 753	88 956	1 640 144
DR4	2015-09-12 2016-06-02	1 551 394	39 498	13 954	96 680	1 701 526
DR5	2016-09-09 2017-06-16	1 226 472	36 093	14 782	119 885	1 397 232
First phase	2011-10-24 2017-06-16	8 171 443	153 090	51 133	642 178	9 017 844

as a DA candidate. Otherwise, it will be classified as non-DA. This algorithm implementation is from SCIKIT-LEARN PYTHON package (Pedregosa et al. 2011), and information of the specific model can be found in their website.[2] Considering the fact that observed spectra, even for the same source, vary from different surveys (i.e. for the same faint source, SDSS spectra are likely to have higher S/N than LAMOST spectra. And SDSS spectra are better flux calibrated, compared to LAMOST spectra etc.), we first built a DA training sample from LAMOST spectra. First of all, there are 379 DA spectra of S/N greater than 10 in SDSS *g* band selected from our previous catalogue (Guo et al. 2015b). Secondly, we randomly selected 100 spectra with the same S/N limit for each spectral type classified by LAMOST pipeline, which is around 6k of non-DA spectra in total. Together, these 379 DA spectra and ∼6k non-DA spectra are used to train the model, then the model is applied to a randomly selected 50k spectra sample for initial test. Based on our test result, most of the contaminants come from A stars. It is understandable, because our RF algorithm mostly uses the broad and deep Balmer line profile of DA stars to select candidates. Some A stars have similar profiles in Balmer line regions. Thus, we added an additional training model specific for separating DA and A stars. The main idea is to distinguish A stars by using their multiple absorption line features in the near-infrared region. Therefore, the largest weight is given to that region. This time, same 379 known DA stars and another 1000 A type star spectra (classified by LAMOST pipeline) with S/N above 10 are selected to train the model. Then this additional model is applied to DA candidates identified by first model. It produces a probability value as well. But this time, if the probability is greater than 50 per cent, this object is classified as A type star. Consequently, its label is changed from DA to non-DA. At last, this code is applied to the whole data set in LAMOST DR 3, 4, and 5. In total, there are 6662 unique spectra candidates selected by our RF algorithm. Each spectrum is visually inspected by eye, 1710 DAs are identified.

In addition, we used a conventional colour-colour cut (Formula 1–4 in Eisenstein et al. 2006, and table 1 in Girven et al. 2011) as supplementary methods to select DAs (see Fig. 1). Even though LAMOST is basically a spectroscopic survey, there are imaging surveys like XSTPS-GAC and SDSS, providing *g*, *r*, and *i* magnitudes for more than 50 per cent of the input catalogue entries. Around 1.46 million entries in LAMOST DR 3, 4, and 5 have *u*, *g*, *r*, *i*, and *z* magnitudes, mostly from SDSS. Using method from Eisenstein et al. (2006), 43 461 WD candidate spectra are selected, whilst 847 DA star candidate spectra are selected adopting method from Girven et al. (2011). For pipeline selection, we select spectra that are classified by the pipeline as WD, WDMagnetic, DoubleStar, or CarbonWD as DA candidates. Spectral types of WDMagnetic, DoubleStar, and CarbonWD are also included, because small number of DA can be misclassified by the pipeline and identification of those types of WD is a part of our goals as well. Those methods result in 6662 unique candidate spectra from RF algorithm, 43 461 candidate spectra from Eisenstein et al. (2006), 847 DA candidate spectra from Girven et al. (2011), and 7024 DA candidates from pipeline selection. In total 2620 bona fide DA spectra and many various types of WDs are identified after visual inspection (See Table 2 and Fig. 2). After cross-matching with the literature, 393 DAs are new identifications (Kleinman et al. 2004, 2013; Zhao et al. 2013; Zhang et al. 2013; Guo et al. 2015b; Kepler et al. 2015, 2016, 2019).

One should note that our strategy in selecting DA stars is to include as many DAs as possible with manageable candidate size. This may result in considerable contamination rate, but rely on visual inspection, contaminants are able to be removed and a relatively complete DA sample can be obtained. Thus, we emphasize the importance of visual inspection of candidate spectra in this work. According to our identification, the efficiency (defined as the ratio of correctly identified DAs to the total number of objects identified as DA candidates) of LAMOST pipeline is $2234/7024 = 31.8$ per cent.

Table 2. Classification for the 3522 spectra of 3069 sources.

Type	Spectra	Sources
DA/DA:	2625	2281
DB/DB:	182	166
DC/DC:	62	58
DCA/DCQ	2	2
DAH/DBH/DAP	34	31
DZ/DZ:	36	33
DZA/DZB	6	4
DAZ/DAZe	6	5
DBAZ/DBAZ:	3	2
DBZ/DBZA	7	4
DAB/DBA/DBA:	76	64
DO/DAO/DOA/DBOA[a]	23	20
DQ/DQ:	19	19
CV/CV:	130	106
(DA,DB,DC,DAH,DBA)+M/DA + (K,DQ)[b]	311	274

Spectral types listed in this paper followed the definitions in Section 2.2 from Kepler et al. (2019).
Especially, notation ':' means uncertainty mainly due to low S/N.
Notation 'e' means emission line present in the spectrum.
[a]DBOA type means its a Helium dominated WD with He II 4 686 Å line and mild Balmer absorption lines.
[b]WD binary. WD with M, K type star or DQ WD.

[2]https://scikit-learn.org/stable/modules/generated/sklearn.ensemble.RandomForestClassifier.html

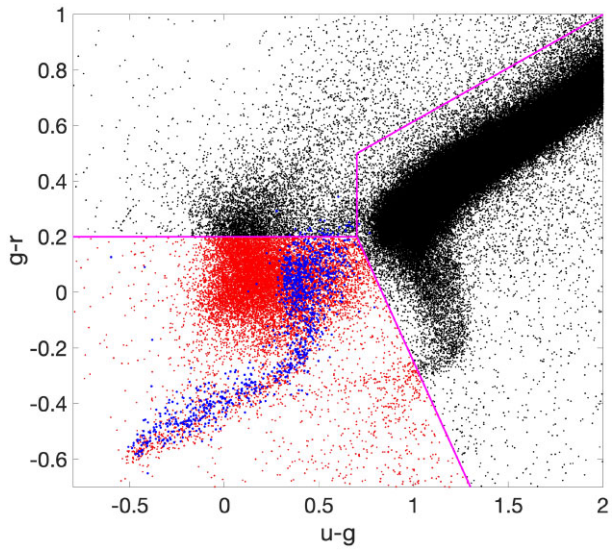

Figure 1. The colour-colour cut selection, based on SDSS *u*-*g* and *g*-*r*, dereddened. The black dots are LAMOST sources with *u*, *g*, and *r* magnitudes, whilst red dots are WD candidates selected following Eisenstein et al. (2006), blue dots are DA stars selected following Girven et al. (2011). Magenta lines have separated different regions defined by Eisenstein et al. (2006). Bottom left is WD candidate region, whilst right region is main-sequence and blue horizontal branch region. Black dots above the horizontal magenta line are mostly quasars.

But more accurately, there are 3869 spectra classified by LAMOST pipeline as DA (i.e. subclass WD). Spectra classified as subclass WDMagnetic and DoubleStar are also included in pipeline method to ensure Magnetic WDs and WDMS binaries are included in our main catalogue. Therefore, the actual efficiency of LAMOST pipeline should be $2234/3869 = 57.7$ per cent. The main contaminants are low S/N spectra. Of the 3869 spectra classified as subclass WD, only 928 spectra have S/N greater than 5 in *u*, *g*, *r*, *i*, and *z* bands. Substantial type A and F stars with very noisy spectra have been wrongly matched with DA templates. The efficiency of RF algorithm is $1\,710/6\,662 = 25.7$ per cent. Similarly, the main contaminants are still A stars (3645 of 6662), together with some F stars and hot subdwarfs. Even though the efficiency of Eisenstein colour cut is only $1172/43\,461 = 2.7$ per cent, majority of other WD types (except DA and DB) are identified through this method. Contaminants are various, more than half of the candidates selected by Eisenstein colour cut method are QSOs, along with B, A, F stars and other types of WDs. The efficiency of Girven colour cuts is $373/847 = 43.9$ per cent. The main contaminants are type G, A, B stars and QSOs. There are 216 DAs missed by LAMOST pipeline and RF algorithm. After a closer look at those DAs, about 100 DAs are found to be misclassified by pipeline as A stars mostly, and B, F stars. Those DAs display relatively narrow absorption lines, compared to the majority of DAs. But they are indeed located in the WD region in the colour-colour plot and *Gaia* colour-magnitude diagram. This indicates the DA templates used by LAMOST pipeline lack low mass DAs. Same problem exists in the RF method, since its training sample is based on our previous catalogue, and identification of low mass DA is generally difficult before *Gaia*. Apart from those 100 missed DAs, another 100 missed DAs have very low S/N spectra (S/N<5 in all SDSS bands). It appears that broad absorption line features in those very noisy spectra have not been picked up by template matching and RF algorithm.

Regarding the completeness ratio of our identified DA sample to all DAs observed by LAMOST, we applied simple and rough ways to estimate, aiming to evaluate the robustness of our DA identification methods. From four methods, LAMOST pipeline identified 2234 DA spectra, two colour cut methods identified 753 spectra, and RF algorithm identified 1710 spectra. Most DA spectra are discovered by two or more methods. Because there is no independent LAMOST imaging survey, substantial LAMOST sources have no required colour to perform the selection, DA spectra identified via colour cut method is highly incomplete. Therefore, only pipeline and RF algorithm identified DAs are used to estimate the completeness. There are 1819, 1523, and 2106 DA spectra with S/N no less than 5 in *g* band identified by LAMOST pipeline, RF method and four methods combined, respectively. The number of common spectra identified by both pipeline and RF is 1379. Thus, the percentage of pipeline missed DA spectra is about $(2106 - 1819)/1819 = 18$ per cent. Since pipeline and RF together identified 1963 unique DA spectra, the percentage of pipeline, and RF missed spectra is about $(2106 - 1963)/1963 = 7$ per cent. Therefore, the total missed DA spectra could be 2106×18 per cent $+ 2106 \times 7$ per cent $= 527$, which means a lower limit of completeness should be around $2106/(2106 + 527) = 80$ per cent. With the help of pipeline and RF method, we managed to identify 1963 DA spectra with S/N no less than 5 in *g* band, which means an upper limit of completeness of pipeline and RF combine is $1963/2106 = 93$ per cent. In summary, the completeness ratio of identified DA sample to all DAs observed by LAMOST is in the range of 80 per cent to 93 per cent. It shows the estimated completeness is consistent, both indicate the number of DA spectra that are not included in our catalogue is not significant.

Another separate test has been carried out by cross matching LAMOST DR 3, 4, and 5 spectra with most recently published SDSS DR 14 DA catalogue first (Kepler et al. 2019), there are 272 DA common sources with S/N ratio no less than 5 in *u*, *g*, and *r* band. Then those sources were cross matched with our DA catalogue, five spectra were found to be missing in our DA catalogue. Therefore, the completeness estimated this way is $5/272 = 98$ per cent, consistent with our previous estimation. Note that those five missed sources were added to our catalogue, making the total number of identified DA spectra 2625.

To further illustrate the ability of different methods in identifying DA spectra as a function of S/N, Fig. 3 is here to show the statistics of DA spectra identified by LAMOST pipeline and RF versus S/N of LAMOST spectra in SDSS *g* band. DA spectra identified by colour cut methods are not considered here as their sample are biased by lacking photometric data. All panels have shown that pipeline method are better than our RF method in identifying more DA spectra and yielding less contaminants, regardless of S/N. Bottom panel indicates that pipeline method yields much more contaminants at low S/N than at high S/N, whilst the contamination rate of RF method seems not much affected by S/N of LAMOST spectra. None the less, more than 60 per cent of RF method selected candidates are contaminants.

2.3 DB selection

Because there are no DB templates in the model database of LAMOST classification pipeline, we only applied RF machine learning method to identify DB stars.

There are 1842 objects in SIMBAD that are listed as DB stars. Those known DBs in SIMBAD were cross-matched with all spectra from LAMOST DR5, resulting in 178 matches, where 150 of these

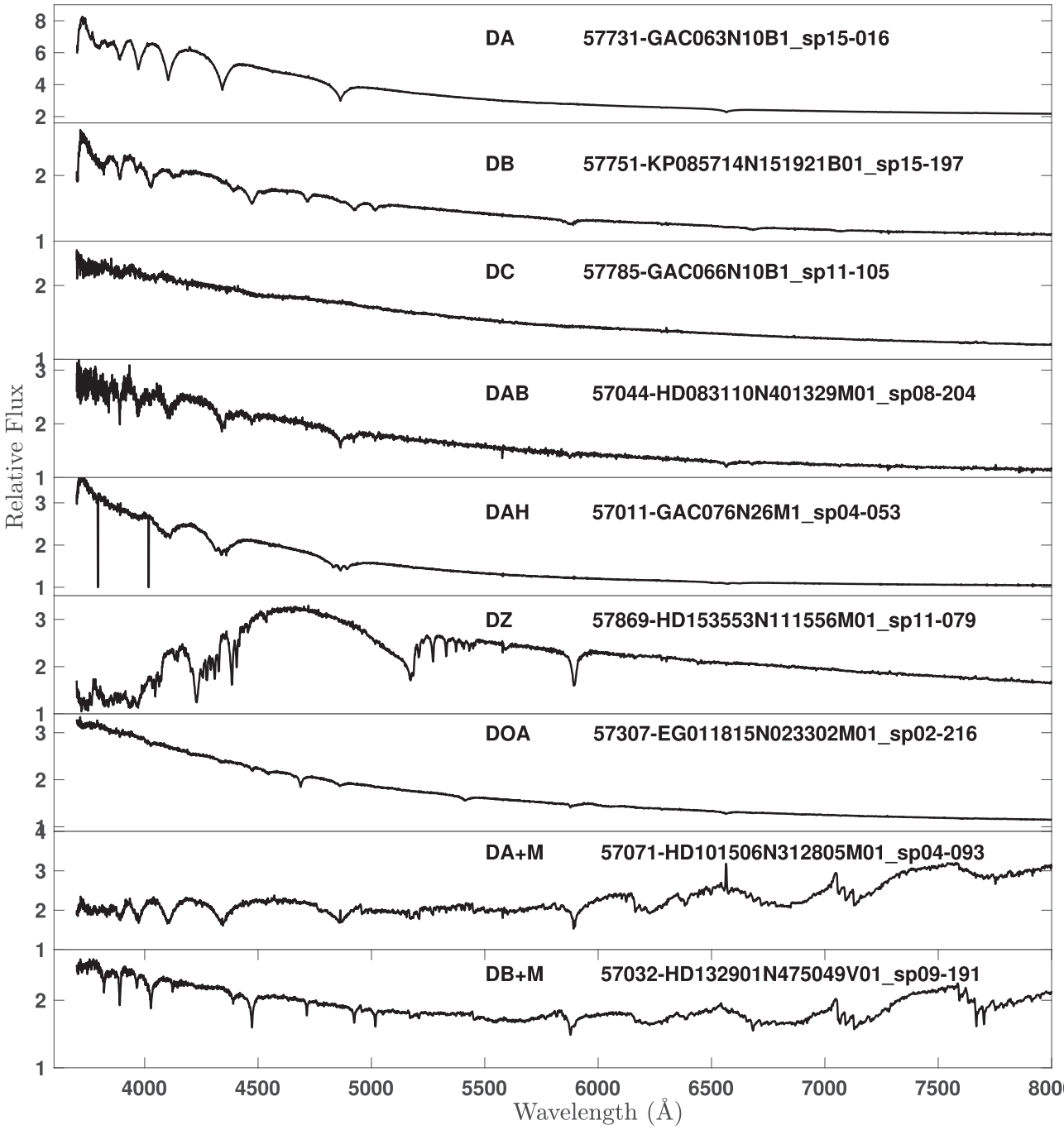

Figure 2. Examples of various WD spectral types identified in LAMOST. In order to focus on the relevant spectral features, this figure only shows the wavelength range 3500–8000 Å. Classified types and their unique LAMOST spectral IDs are also shown.

are classified as UNKNOWN by LAMOST pipeline. A large portion of those 150 spectra have very low S/N ratio that are not able to be identified by eyes. Thus, 58 of 178 known DBs are not recovered by our DB selection. Because we can not identify them based on their unrecognizable noisy LAMOST spectra alone, and these noisy spectra have no use for any analysis, those are not included as DBs in this paper. In order to select a high-quality sample to best represent DB features, we only chose those LAMOST spectra with S/N >10 in the SDSS g band. There are 45 spectra that meet this criterion and form the training sample. Next, after removal of the 178 known SIMBAD DB spectra, roughly 1000 spectra with S/N>10 were randomly selected from LAMOST DR5. Most of those 1000 spectra are different types of star, together with galaxies and QSOs. DB spectra are ensured to be excluded by careful spectral inspections. Similar to RF method applied to identify DAs, we used all unsmoothed 45 DB and $\sim$1000 non-DB spectra to construct the supervised DB classifier for the RF algorithm. All flux values of a spectrum are adopted as parameters. The largest weight is given to parameters in the region of Helium absorption line wings. A simple DB or non-DB classification is used. An object is classified

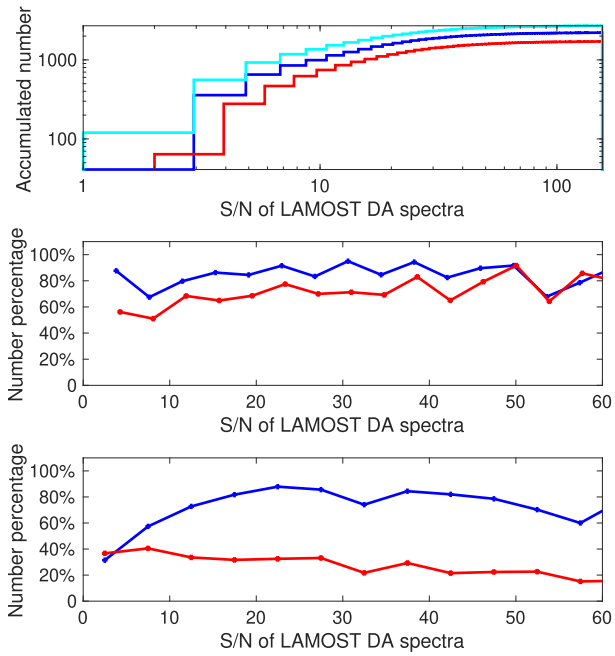

Figure 3. The statistics of DA spectra number identified by different methods as a function of S/N in SDSS *g* band. Top panel: accumulated number histograms of LAMOST pipeline, RF algorithm, and all methods identified DA spectra in blue, red, and cyan colour, respectively. Middle panel: number percentage of LAMOST pipeline (blue line) and RF algorithm (red line) identified DA spectra in all DA spectra identified as a function of S/N. Bottom panel: blue line represents number percentage of LAMOST pipeline identified DA spectra in candidate spectra selected by pipeline, whilst red line represents number percentage of RF algorithm identified DA spectra in candidate spectra selected by RF method.

as a DB candidate, when its probability of being DB star is greater than 50 per cent. Or this object will be classified as non-DB. In the final step, all spectra in DR 3, 4, and 5 are fed to the classifier, DB candidates are obtained.

There are 12 572 DB candidates selected by the RF algorithm. After visual inspection, 182 spectra of 166 sources were found to be bona fide DBs. After cross-matching with previous published catalogues, 46 DBs are new identifications (Kleinman et al. 2004, 2013; Kepler et al. 2015, 2016; Guo et al. 2015b). We believe that higher contamination rate in DB selection is caused by smaller training sample size relative to DA training sample. In addition, a second training is applied to distinguish DA and A star in DA machine learning selection.

2.4 Other WD spectral types

Besides DA and DB stars, other spectral types of WD are identified as well, as a result of our effort in searching for DA stars. They are from the colour-colour cut selection method from Eisenstein et al. (2006), Girven et al. (2011), and visual inspection of spectra that are classified as WDMagnetic, DoubleStar, and CarbonWD. Colour-colour cut from Eisenstein et al. (2006) yielded more types of WD than any other methods. But not all LAMOST sources have SDSS photometry, so WD types except DA and DB are highly incomplete.

There are five DAZs, four DBZs, and two DBAZs identified in this work. Two of five DAZs are classified as WD by LAMOST pipeline, Three of four DBZs and one of two DBAZs are selected as DB candidates by RF algorithm. The rest $3 + 1 + 1 = 5$ are discovered by Eisenstein's colour cut method. Based on a rough estimation, the fraction of those special metal polluted WDs in Eisenstein's colour cuts selected WD candidates is about $5/43\,461 = 0.011$ per cent, and the fraction of this colour cuts selected candidates in LAMOST DR3, 4 & 5 that have SDSS photometry is $43\,461/1\,455\,566 = 2.98$ per cent. Therefore, the number of those special WDs that have been missed in LAMOST because they do not have SDSS photometry is $(4\,740\,458 - 1\,455\,566) \times (0.011$ per cent $\times\ 2.98$ per cent$) \approx 11$. Besides those three types of WDs, magnetic WDs (DAH, DBH, and DAP) mainly come from pipeline classified WDMagnetic, whilst pipeline classified DoubleStar identified most WDMS binaries and CVs. And all the spectral types identified in this work with their corresponding numbers are listed in Table 2. A small part of basic parameters of all WDs identified in LAMOST DR 3, 4, and 5, including designation, RA, Dec., observation date, unique spectral ID, and WD subtype, has shown in Table 3.

3 PARAMETER DETERMINATION

3.1 $T_{\rm eff}$ and log *g* for DA stars

In order to ensure the accuracy of the derived parameters for DAs, only spectra with S/N >15 in SDSS *g* band are fitted. For sources with multiple observations, those with highest *g* band S/N are used. To estimate the effective temperature and surface gravity of DA stars, absorption line profiles from Hβ to Hϵ were fitted to theoretical spectral models. Before performing the spectral fitting, both the observed and model absorption line profiles were trimmed and normalized following standard procedures (Liebert, Bergeron & Holberg 2005). The next step is to use a minimization technique to fit the line profile. The technique adopted here is the well known non-linear least-squares method of Levenberg-Marquardt, which is based on a steepest descent method. To fit the best model template, the open source IDL package MPFIT was used (Markwardt 2009). The DA atmosphere models used here are provided by Koester (private communication) and are based on those described in Koester (2010). The errors for $T_{\rm eff}$ and log *g* were determined by stepping the parameters about the minimum χ^2. The difference, which is calculated between each current minimum χ^2 and the previous true minimum χ^2, corresponds to 1σ for a given number of free model parameters is regarded as the error.

Notably, we introduced *Gaia* $G_{\rm BP}$-$G_{\rm RP}$ colour into the spectral fitting process. First, a sample of SDSS identified DAs with relatively high precision $T_{\rm eff}$ is constructed. Next, an empirical relation is established between $T_{\rm eff}$ and their corresponding *Gaia* colour. Then for a new DA spectrum to be fitted, an initial effective temperature value was given by the empirical relation, based on its *Gaia* colour. The initial value was then used as one input parameter in MPFIT code to start model fitting iterations (More details in Zhang et al. [in prep]). After this preparation, it's the same pure conventional spectral fitting to theoretical model spectra to obtain the final $T_{\rm eff}$ and log *g*. By using *Gaia* data in this way, the final effective temperature will be determined more robustly and accurately than our previous study (Guo et al. 2015b). Two examples of Balmer line fitting are shown in Fig. 4. For comparison purposes, we chose one spectrum with high S/N (J041010.37+180222.8), and another spectrum with low S/N (J071004.93 + 292403.2). Fig. 5 shows a χ^2 contour plot of $T_{\rm eff}$ and log *g* for the source J041010.37 + 180222.8. The best-fitted values for $T_{\rm eff}$ and log *g*, together with their uncertainties are estimated from the minimum converged residual χ^2. The median error of $T_{\rm eff}$ and log *g* in our DA sample is roughly 8 per cent and 4 per cent, respectively.

Table 3. Basic parameters of WDs from LAMOST DR 3, 4, and 5. Only part of the catalogue is shown here. The full table can be found in the supplementary material.

GID[a]	ObsID[b]	Designation[c]	RA	DEC	Obs-date[d]	Mjd-Planid_spid-Fiberid[e]	Type
1_2	247515227	J002633.24 + 390902.9	6.638503	39.150817	2014-09-10	56911-HD002951N381926B01_sp15-227	DAZ
1_2	354311163	J002633.13 + 390904.0	6.6380824	39.151121	2015-09-14	57280-M31007N36M1_sp11-163	DAZ
2_2	249301140	J041010.37 + 180222.8	62.543227	18.039691	2014-09-26	56927-GAC062N19B1_sp01-140	DA
2_2	318401139	J041010.37 + 180222.8	62.543227	18.039691	2015-02-13	57067-GAC062N19B2_sp01-139	DA
3_2	250301120	J042355.72 + 162113.2	65.982207	16.353693	2014-10-05	56936-GAC065N18B1_sp01-120	DA
3_2	250401120	J042355.78 + 162114.9	65.982452	16.354149	2014-10-05	56936-GAC065N18B2_sp01-120	DA
4_2	250407081	J042839.47 + 165811.7	67.164496	16.969927	2014-10-05	56936-GAC065N18B2_sp07-081	DA
4_2	420109239	J042839.40 + 165812.0	67.1642003	16.9700186	2016-02-05	57424-KP042325N164638B01_sp09-239	DA
5_2	252902097	J024746.29 + 000331.6	41.942909	0.0587914	2014-10-13	56944-EG025338N015809M01_sp02-097	DA
5_2	367416195	J024746.39 + 000331.1	41.943312	0.058658	2015-10-08	57304-EG025335S013827B01_sp16-195	DA
6_2	252908132	J025817.87 + 010946.0	44.574461	1.1627782	2014-10-13	56944-EG025338N015809M01_sp08-132	DA + M
6_2	300710119	J025817.87 + 010946.0	44.574461	1.1627782	2015-01-20	57043-EG030739N012421M01_sp10-119	DA + M
7_3	254115228	J040342.10 + 145928.7	60.9254278	14.9913211	2014-10-15	56946-HD040531N141710B01_sp15-228	DA
7_3	381910034	J040342.21 + 145929.8	60.925876	14.991617	2015-11-03	57330-GAC062N15B1_sp10-034	DA
7_3	382010034	J040342.19 + 145928.4	60.925814	14.991239	2015-11-03	57330-GAC062N15B2_sp10-034	DA
8_2	256106072	J225745.89 + 074320.5	344.44124	7.722373	2014-10-25	56956-EG224840N075042M01_sp06-072	DA
8_2	380401098	J225745.89 + 074320.5	344.44124	7.722373	2015-11-01	57328-EG225829N094931M01_sp01-098	DA
9_2	256113149	J225605.44 + 081936.3	344.0227	8.32677	2014-10-25	56956-EG224840N075042M01_sp13-149	DA
9_2	380402065	J225605.44 + 081936.3	344.0227	8.32677	2015-11-01	57328-EG225829N094931M01_sp02-065	DA
10_2	256201054	J055944.97 + 171203.3	89.937392	17.20094	2014-10-25	56956-GAC090N18M1_sp01-054	DA
10_2	420409046	J055944.97 + 171203.4	89.937412	17.200946	2016-02-06	57425-GAC089N16M1_sp09-046	DA
11_2	256601015	J061518.94 + 153059.4	93.828958	15.5165	2014-10-26	56957-GAC093N17M1_sp01-015	CV
11_2	400112059	J061518.94 + 153059.4	93.828958	15.5165	2016-01-04	57392-GAC092N13M1_sp12-059	CV
12_2	257606145	J071004.93 + 292403.2	107.52056	29.400907	2014-11-01	56963-GAC105N29B1_sp06-145	DA
12_2	281116178	J071004.93 + 292403.2	107.52056	29.400907	2014-12-18	57010-GAC108N27B1_sp16-178	DA
13_3	259201037	J075853.02 + 161645.1	119.72092	16.279214	2014-11-04	56966-GAC120N18B1_sp01-037	CV
13_3	392716175	J075853.02 + 161645.1	119.72092	16.279214	2015-12-21	57378-GAC120N14B1_sp16-175	CV
13_3	392816175	J075853.02 + 161645.1	119.72092	16.279214	2015-12-21	57378-GAC120N14B2_sp16-175	CV
14_2	265114068	J060911.91 + 352549.3	92.299661	35.430376	2014-11-12	56974-GAC094N35B1_sp14-068	DA
14_2	385314070	J060912.00 + 352549.1	92.300011	35.430329	2015-12-01	57358-GAC094N35B2_sp14-070	DA
15_2	266807242	J022301.66 + 061649.5	35.756946	6.2804389	2014-11-16	56978-EG021841N081050M01_sp07-242	CV
15_2	474703167	J022301.66 + 061649.5	35.756946	6.280439	2016-11-02	57695-EG022616N061733M01_sp03-167	CV

[a] Group ID. i.e. '1_2" means group 1 has 2 spectra.
[b] Observation ID, which is also unique for each spectrum.
[c] Designation from LAMOST. The exact number could be slight different for the same group.
[d] Observation date of the spectrum.
[e] Unique spectrum ID.

3.2 $T_{\rm eff}$ and log g for DB stars

To ensure the number of DB stars with parameters that can be compared with the literature, we adopt a S/N limit of 10. The DB spectrum with highest S/N was chosen for model fitting in the case that a source has multiple spectra. Also, because there can be a large number of helium absorption lines, the fitting process is complicated by their normalization. Therefore, the parameter determination for DB spectrum is usually done by fitting the entire spectrum to the theoretical model. But in this case, flux calibration errors may affect the accuracy of parameter estimation. Flux calibration is difficult for LAMOST spectra, owing to e.g. flat-fielding over large fields of view, use of pseudo-standard stars, and possible unknown reddening (Du et al. 2016). To evaluate which is more suitable for LAMOST DB spectral fitting, by fitting only Helium absorption lines after continuum normalization (similar to DA spectral fitting) or fitting the entire flux calibrated spectrum directly, a sample of a few tens of known DB stars from Koester & Kepler (2015) is selected to perform a less formal test. Those DB stars are common sources of our LAMOST DB sample and DB catalogue from Koester & Kepler (2015) with relatively small errors of derived $T_{\rm eff}$ and log g. Two sets of parameters are derived from these two different methods, who performed on LAMOST spectra. Next, both results were compared with SDSS catalogue values, and we found that fitting the entire flux calibrated spectrum yielded more consistent results. Therefore, we chose this method despite flux calibration concerns. The DB models used in the fits were pure He models, kindly provided by Koester (2010). Fig. 6 shows two examples of DB stars where the entire spectra were fitted by models. One is DB spectrum with high S/N (J164718.38 + 322832.8, S/N=57), whilst the other has lower S/N (J012148.23-001053.0, S/N = 29). The best-fitted $T_{\rm eff}$ and log g, as well as their uncertainties are also obtained from the minimum converged residual χ^2. It is noted that the effective temperature and surface gravity for DB training sample we adopted ranges from 11 722 to 33 894 K and 7.6 to 8.7 dex, respectively, according to SIMBAD records. Therefore, even though these ranges should cover most of DB stars, it is still possible that a small number of DBs with $T_{\rm eff}$ and log g outside these ranges are missing in our DB catalogue.

3.3 Mass and cooling age

Once the $T_{\rm eff}$ and log g are obtained from the model fitting, their mass, and cooling age can be estimated based on evolutionary models

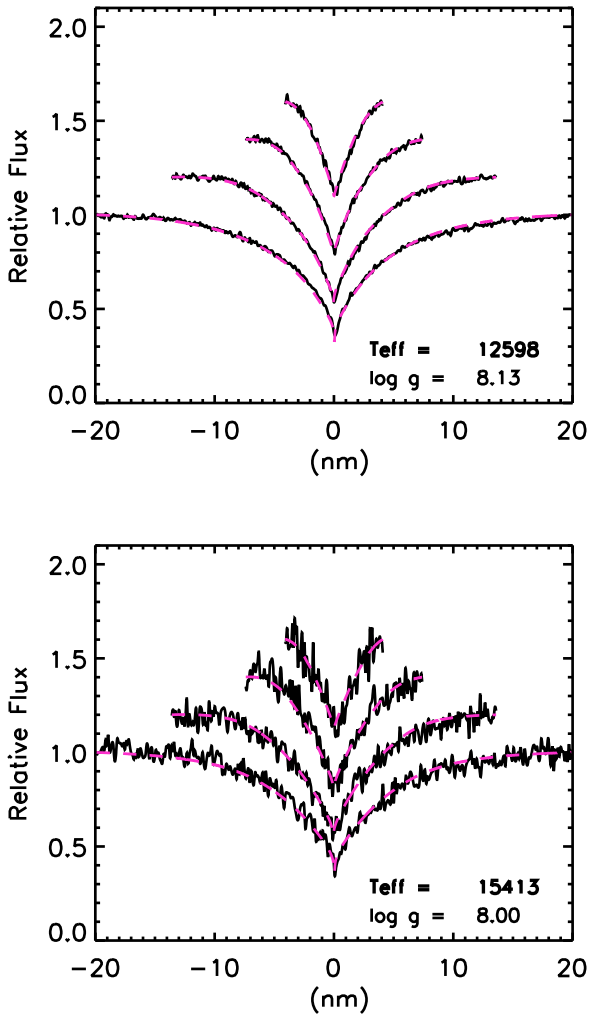

Figure 4. Balmer line fitting examples for J041010.37+180222.8 (upper panel, S/N=107) and J071004.93 + 292403.2 (lower panel, S/N = 28). For both cases, the black solid lines are observed and normalized DA spectra, whilst red dashed lines are the best-fitting model. From bottom to top of each panel, fitted absorption lines are H β, H γ, H δ, and H ϵ, respectively.

(Fontaine et al. 2001).[3] For DAs, the cooling models in Wood (1995) was used for the carbon-core with thick ($q_{\rm H} = M_{\rm H}/M_{\star} = 10^{-4}$) hydrogen layers with $T_{\rm eff}$ greater than 30 000 K. For models with effective temperature less than 30 000 K, the cooling models for carbon-oxygen cores in Fontaine et al. (2001) with thick ($q_{\rm H} = 10^{-4}$) hydrogen layers are used. For DBs, the cooling models in Wood (1990) was adopted for the carbon-core with thick ($q_{\rm He} = M_{\rm He}/M_{\star} = 10^{-4}$) helium layers (Bergeron, Leggett & Ruiz 2001).

An example of mass and cooling age determination is demonstrated in Fig. 7. The resulting distributions of mass and cooling age are shown in Figs 8 and 11, respectively. There are 1316 DAs and 70 DBs with good quality spectra that can be used to construct these distributions.

Looking at Fig. 8, the DA mass range is from 0.3 to 1.2 $M_{\odot}$, with a peak near 0.62 $M_{\odot}$. This is in agreement with the mean mass of 0.613 $M_{\odot}$ from Tremblay, Bergeron & Gianninas (2011) and our

[3]The cooling model can be downloaded from the Web site: http://www.astro.umontreal.ca/~bergeron/CoolingModels/.

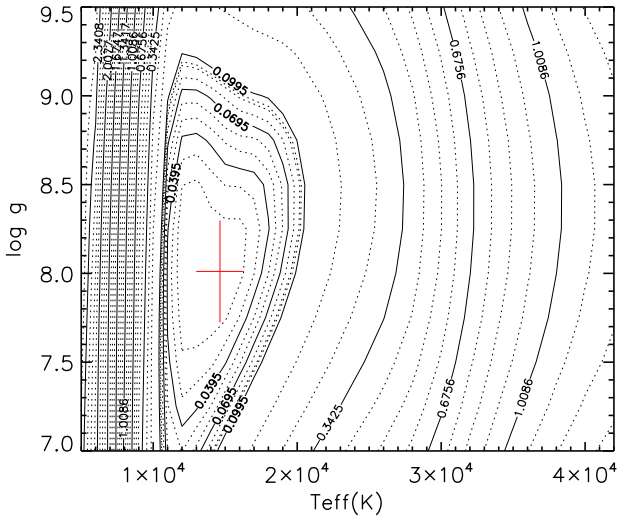

Figure 5. χ^2 contour plot of $T_{\rm eff}$ and $\log g$ determination for DA J041010.37 + 180222.8. Red cross represents final result with its uncertainties.

previous research (Guo et al. 2015b). But our peak mass is slightly less massive than the mean mass of 0.649 $M_{\odot}$ from Kepler et al. (2015). As is well established in the literature (and references therein Rebassa-Mansergas et al. 2015) as well as in Guo et al. (2015b), two obvious, non-single Gaussian distribution features present near 0.4 and 1.0 $M_{\odot}$. However, these features are not evident in our combined DA mass distribution of DR 1–5.

Of all the fitted LAMOST DAs, 506 stars are found to have fitted parameters in the SDSS DR14 WD catalogue (Kepler et al. 2019). In Fig. 9, we compare our results with Kepler et al. (2019). In general, both sets of results are in good agreement. Sources common to both studies with higher S/N LAMOST spectra exhibit higher consistency between the studies. Also, the derived surface gravities and thus corresponding masses are more discrepant at the high and low ends. Our study systematically underestimates masses at the high end, and overestimates mass at the low end, relative to the SDSS WD study. In terms of S/N, the difference is displayed clearly in the bottom panel of Fig. 9. Regarding DAs with LAMOST spectra S/N of less than ~50, the SDSS spectra quality are obviously better than LAMOST spectra. However, as for DAs with LAMOST spectra S/N of greater than 50, the LAMOST spectra quality are clearly better. We suggest our derived parameters are reliable for S/N above 30. Similarly, there are 1059 stars found to have fitted parameters in the *Gaia* DR2 WD catalogue (Gentile Fusillo et al. 2019). In Fig. 10, our parameters and results from Gentile Fusillo et al. (2019) are compared. Results from both catalogues are generally agreed with each other. However, the derived surface gravity and mass data are clearly more disperse than the data from comparisons between LAMOST and SDSS, despite S/N of LAMOST spectra. It is understandable that parameters like surface gravity and mass derived from spectral fitting are generally more accurate and reliable. Moreover, derived $T_{\rm eff}$ from *Gaia* are much more consistent with LAMOST $T_{\rm eff}$ when they are low. This implies derived $T_{\rm eff}$ from *Gaia* for relatively cool WDs are generally reliable, whilst for hotter WDs, derived $T_{\rm eff}$ should be used cautiously.

With respect to the parameter distributions of the 70 relatively high S/N DBs, the peak in mass is located near 0.65 $M_{\odot}$, and the peak in $\log g$ distribution is around 8.0 (Fig. 11). These distributions are consistent with the literature (Eisenstein et al. 2006; Kleinman

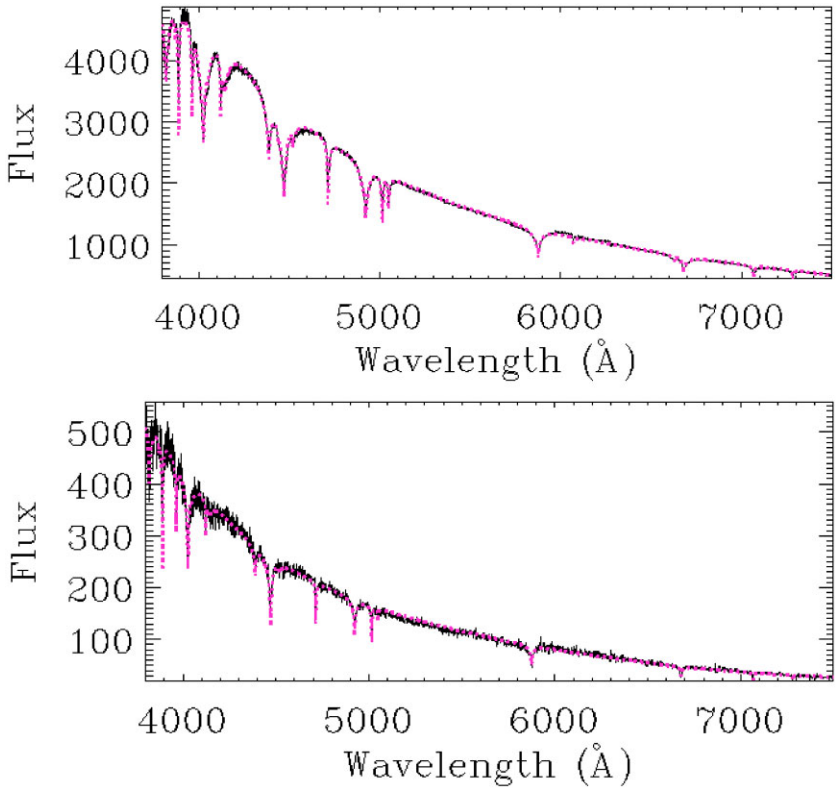

Figure 6. DB Helium absorption lines model fit comparison between J164718.38 + 322832.8 (upper panel, S/N=57) and J012148.23-001053.0 (lower panel, S/N = 29). The black solid lines are observed DB spectra, whilst red dashed lines are best-fitting model spectra.

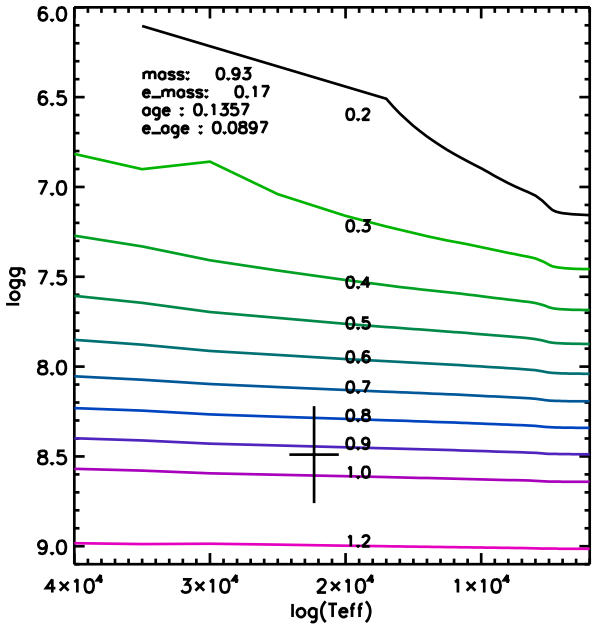

Figure 7. One example of mass and cooling age determination, based on effective temperature and surface gravity. Black cross represents the location of this example with uncertainties in the effective temperature versus surface gravity space. Different lines represent theoretical models with correspondent mass. Determined mass and cooling age are shown in the upper left with their errors.

et al. 2013). It is difficult to draw any further conclusions from these distributions, because there are so few sources.

Amongst the 70 DBs with derived parameters, 42 have parameters in Kleinman et al. (2013) and Koester & Kepler (2015), but only 11 sources have derived masses. In Fig. 12, from top to bottom panel, these are comparisons of mass, effective temperature, surface gravity, and S/N between our results and results from Kleinman et al. (2013) and Koester & Kepler (2015), respectively. Based on these direct comparisons, our results are generally consistent with results from SDSS. It is also true that DBs with higher S/N tend to have more consistent parameters than DBs with lower S/N. And SDSS DB spectra have higher S/N than SDSS spectra, when the S/N of LAMOST DBs are less than ∼50. Even though there are only three sources, it's likely the opposite when the S/N of LAMOST DBs are greater than ∼50.

4 ON GOING AND FUTURE WD CANDIDATE SELECTION FOR LAMOST

We have been selecting potential WD targets for future, low-resolution, and LAMOST spectral fibre selection. In this section, we describe our pre-*Gaia* DR2 criteria for the second phase survey. Even though with the release of *Gaia* 2nd data release, a WD candidates sample as large as 486 641 has been revealed (Gentile Fusillo et al. 2018), and their $T_{\rm eff}$, $\log g$, radii, and mass can be inferred from accurate photometry and trigonometric parallax. However, the importance of obtaining the optical WD spectra can not be neglected. One important application is to discover more rare WDs with emission lines caused by gaseous debris disc or

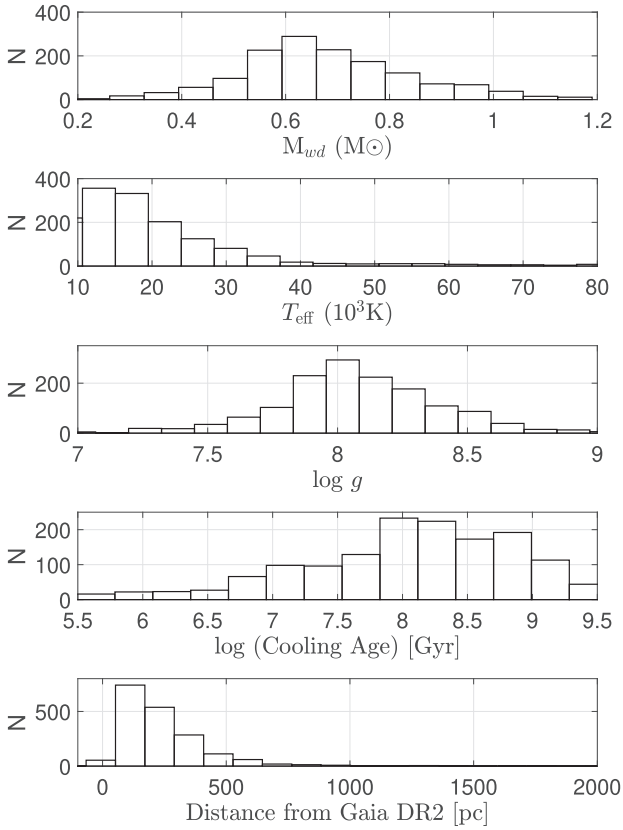

Figure 8. Distributions of derived DA parameters, including DAs with updated parameters from LAMOST DR2. From top to bottom: mass, effective temperature, surface gravity, cooling age, and inverted parallax from Gaia DR2.

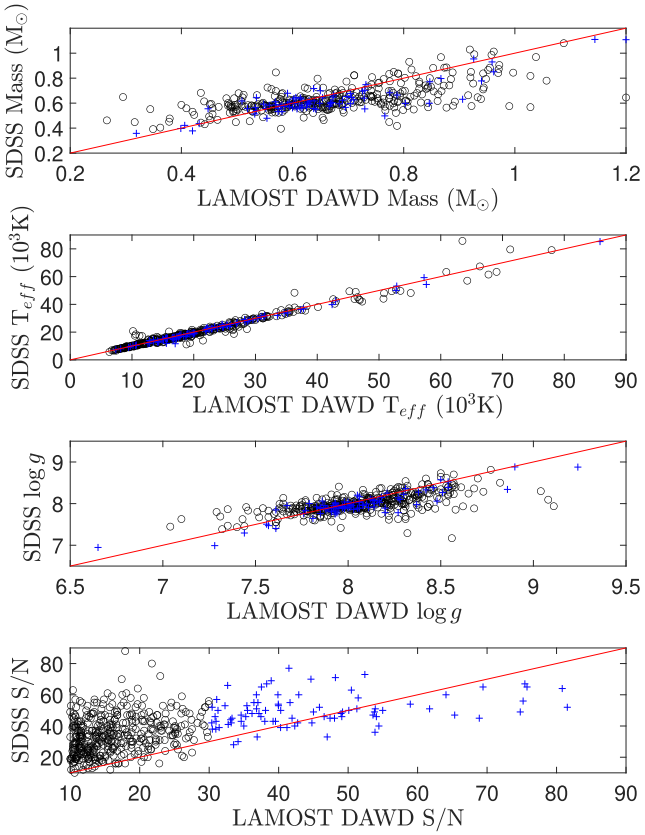

Figure 9. Comparisons between LAMOST DA parameters (DAs with updated parameters from LAMOST DR2 are also included) and SDSS parameters from Kepler et al. (2019). From top to bottom: mass, effective temperature, surface gravity, and S/N. Black circles represent DAs with S/N of LAMOST spectra between 10 and 30, whilst blue crosses are DAs with S/N of LAMOST spectra greater than 30. The red solid lines are unit slope relation.

irradiation from unseen substellar object (Gänsicke et al. 2006; Melis et al. 2012; Guo et al. 2015a; Manser et al. 2019). Another example is to identify more metal polluted WDs (DZs), which can be a unique tool to analyse the chemical composition of their tidally disrupted planetesimal (Gänsicke et al. 2012; Farihi, Gänsicke & Koester 2013). As a matter of fact, in order to obtain WD optical spectra, future large multi-object spectroscopic surveys are planning to observe these WD candidates from *Gaia*. For instance, SDSS-V (Kollmeier et al. 2017), 4most (de Jong et al. 2012), WEAVE (Dalton et al. 2012), and DESI (DESI Collaboration 2016).

At the end of the LAMOST first phase survey in 2017 June, we began a process of selecting WD candidates, based on reduced proper motion. The photometric data we used is taken from the XSTPS-GAC (Guo et al. 2018) and Pan-STARRS (Kaiser et al. 2010), whilst the proper motion data are from the Gaia-PS1-SDSS (GPS1 Tian et al. 2017) proper motion catalogue. XSTPS-GAC is a photometric sky survey in the SDSS *gri* bands, and because LAMOST sources are selected from XSTPS-GAC, it is highly suitable for WD candidate identification. The total number of sources in XSTPS-GAC is 110 168 720, and after cross-matching with GPS1 within 3 arcsec, there are 56 059 242 sources in common. It is worth mentioning that this is a simple direct cross-matching without considering the epochs of observations and proper motion of stars. We use equation 1 to calculate reduced proper motion, and plot this against $g - i$ in order to identify WD candidates, where Fig. 13 shows our exact parameter cuts.

Common sources are plotted in the *g*-*i* colour versus RPM space, over-plotted with the density contours. Red triangles represent 2030 known DAs amongst these common sources, whilst blue triangles represent 127 known DBs in the same sample. Based on their location, WDs should locate in the same region. Therefore, we defined a triangle region to separate the WDs and the other types of star. The triangle region is defined by cyan solid line, *x*-axis and *y*-axis. Black dots are common sources located in the defined region, which represent selected WD candidates.

Our reduced proper motion cuts yielded 30 441 WD candidates. Next, we cross-matched these objects with the literature, finding 20 628 sources are previously unrecognized WD candidates (at that time). These candidates were entered into the target selection software designed for LAMOST. Some of those WD candidates have already been observed and included in DR6, whilst the rest will appear in the second phase.

$$RPM = g + 5 \times log(PM) + 5 \quad (1)$$

After the second release of *Gaia* data in 2018 April, Gentile Fusillo et al. (2018) has revealed a WD candidate sample as large as 486 k. Unfortunately, our selection of WDs for LAMOST second phase has completed in 2017. None the less, plan has been made to utilize this high fidelity catalogue to form a proper sample for LAMOST to observe in the future.

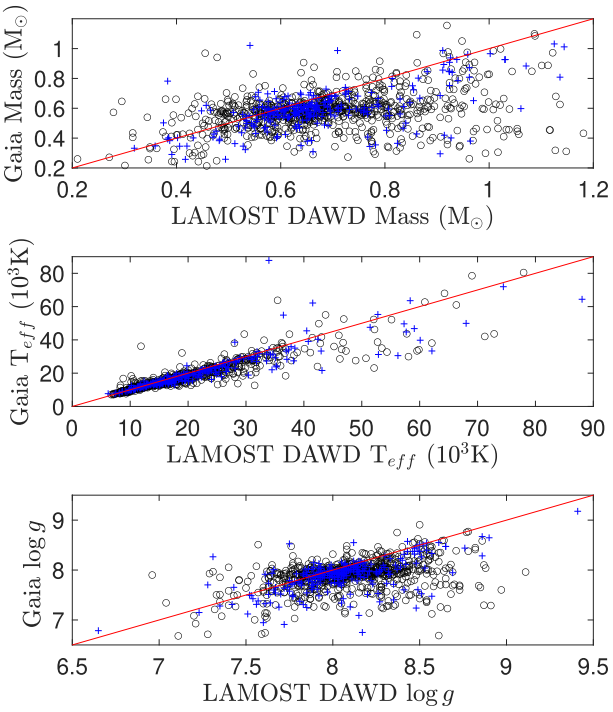

Figure 10. Comparisons between LAMOST DA parameters (DAs with updated parameters from LAMOST DR2 are also included) and *Gaia* DR2 WD parameters from Gentile Fusillo et al. (2019). From top to bottom: mass, effective temperature, and surface gravity. Black circles represent DAs with S/N of LAMOST spectra between 10 and 30, whilst blue crosses are DAs with S/N of LAMOST spectra greater than 30. The red solid lines are unit slope relation.

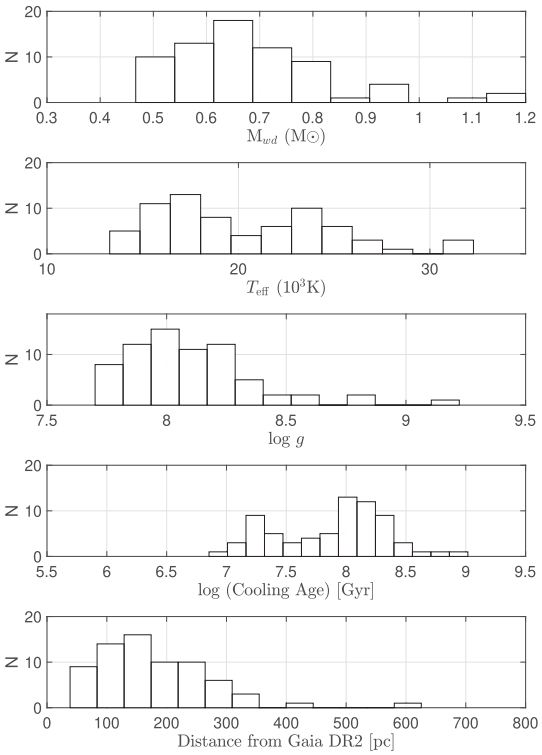

Figure 11. Distributions of derived DB parameters. From top to bottom: mass, effective temperature, surface gravity, cooling age, and inverted parallax from *Gaia* DR2.

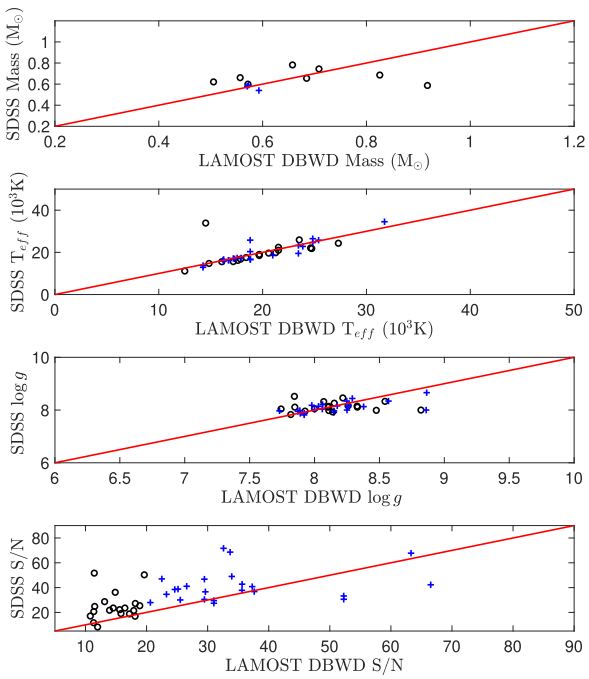

Figure 12. Comparisons between LAMOST DB parameters and SDSS parameters from Kleinman et al. (2013) and Koester & Kepler (2015). From top to bottom: mass, effective temperature, surface gravity, and S/N. Black circles represent DBs with S/N of LAMOST spectra between 10 and 20, whilst blue crosses are DAs with S/N of LAMOST spectra greater than 20. The red solid lines are unit slope relation.

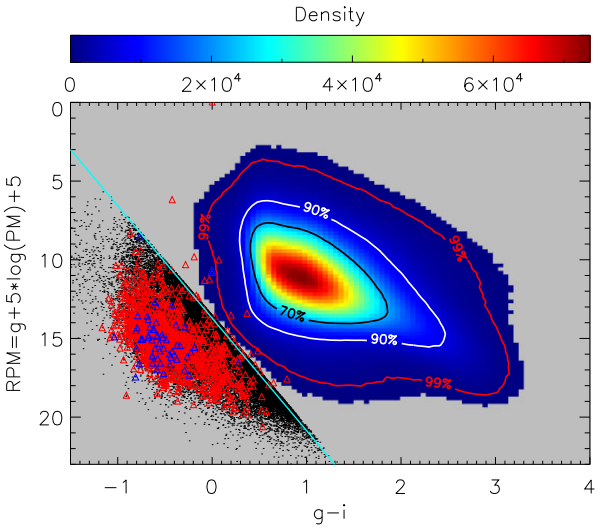

Figure 13. Colour g-i versus RPM. The coloured density map and contours demonstrate the majority of common stars locate at the central region. Red triangles represent known DAs in the common source sample, whilst blue triangles represent known DBs. The cyan solid line is defined to separate WDs from majority of stars. The black dots are selected WD candidates, based on the RPM approach.

Table 4. Determined WD parameters and parameters from Gaia DR2. (Only part of the catalogue is shown here. The full table can be found in the supplementary material.).

GID[a]	ObsID[b]	S/N$_g^c$	$T_{\rm eff}$ (K)	log g	Mass ($M_\odot$)	Age (Myr)	Plx[d] (mas)	PMra[e] (mas/yr)	PMdec[e] (mas/yr)	mag$_G^f$	Type
1_2	247515227	11					15.8342 ± 0.066	142.505 ± 0.102	− 130.002 ± 0.087	15.800	DAZ
1_2	354311163	3					15.8342 ± 0.066	142.505 ± 0.102	− 130.002 ± 0.087	15.800	DAZ
2_2	249301140	105					29.3892 ± 0.0572	72.19 ± 0.14	− 85.906 ± 0.096	14.244	DA
2_2	318401139	124	15312 ± 1369	8.04 ± 0.27	0.64 ± 0.16	199 ± 114	29.3892 ± 0.0572	72.19 ± 0.14	− 85.906 ± 0.096	14.244	DA
3_2	250301120	22					22.2272 ± 0.0519	114.412 ± 0.103	− 27.715 ± 0.079	14.347	DA
3_2	250401120	39	20526 ± 1688	8.24 ± 0.27	0.77 ± 0.17	109 ± 73	22.2272 ± 0.0519	114.412 ± 0.103	− 27.715 ± 0.079	14.347	DA
4_2	250407081	115					20.8952 ± 0.0567	102.692 ± 0.115	− 26.885 ± 0.068	14.074	DA
4_2	420109239	116	26029 ± 1851	8.14 ± 0.29	0.72 ± 0.18	27 ± 4	20.8952 ± 0.0567	102.692 ± 0.115	− 26.885 ± 0.068	14.074	DA
5_2	252902097	9					8.1485 ± 0.0776	130.453 ± 0.136	− 41.637 ± 0.125	16.488	DA
5_2	367416195	35	19475 ± 1519	8.07 ± 0.27	0.66 ± 0.16	92 ± 65	8.1485 ± 0.0776	130.453 ± 0.136	− 41.637 ± 0.125	16.488	DA
6_2	252908132	7								17.818	DA + M
6_2	300710119	5								17.818	DA + M
7_3	254115228	101	14421 ± 2543	8.43 ± 0.27	0.88 ± 0.17	442 ± 283	24.0527 ± 0.0541	141.19 ± 0.107	− 24.07 ± 0.084	15.038	DA
7_3	381910034	53					24.0527 ± 0.0541	141.19 ± 0.107	− 24.07 ± 0.084	15.038	DA
7_3	382010034	42					24.0527 ± 0.0541	141.19 ± 0.107	− 24.07 ± 0.084	15.038	DA
8_2	256106072	7					4.557 ± 0.2331	-15.071 ± 0.374	− 40.83 ± 0.269	18.302	DA
8_2	380401098	12					4.557 ± 0.2331	-15.071 ± 0.374	− 40.83 ± 0.269	18.302	DA
9_2	256113149	6					6.3772 ± 0.1	-19.921 ± 0.199	− 1.312 ± 0.136	16.738	DA
9_2	380402065	37	23254 ± 2294	7.65 ± 0.34	0.47 ± 0.13	20 ± 7	6.3772 ± 0.1	-19.921 ± 0.199	− 1.312 ± 0.136	16.738	DA
10_2	256201054	57					12.713 ± 0.0718	0.726 ± 0.121	− 19.04 ± 0.1	15.841	DA
10_2	420409046	87	18982 ± 1348	8.31 ± 0.25	0.81 ± 0.16	162 ± 98	12.713 ± 0.0718	0.726 ± 0.121	− 19.04 ± 0.1	15.841	DA
11_2	256601015	4					1.2902 ± 0.1754	− 0.069 ± 0.31	− 8.973 ± 0.311	17.961	CV
11_2	400112059	3					1.2902 ± 0.1754	− 0.069 ± 0.31	− 8.973 ± 0.311	17.961	CV
12_2	257606145	19					14.4462 ± 0.0781	− 1.383 ± 0.114	− 101.355 ± 0.102	15.515	DA
12_2	281116178	28	15710 ± 1559	7.97 ± 0.31	0.60 ± 0.17	162 ± 95	14.4462 ± 0.0781	− 1.383 ± 0.114	− 101.355 ± 0.102	15.515	DA
13_3	259201037	43					4.79 ± 0.0572	− 26.015 ± 0.116	− 0.264 ± 0.063	15.515	CV
13_3	392716175	26					4.79 ± 0.0572	− 26.015 ± 0.116	− 0.264 ± 0.063	15.515	CV
13_3	392816175	41					4.79 ± 0.0572	− 26.015 ± 0.116	− 0.264 ± 0.063	15.515	CV
14_2	265114068	16					20.6106 ± 0.0851	− 0.299 ± 0.107	51.212 ± 0.096	15.681	DA
14_2	385314070	33	10214 ± 360	8.39 ± 0.35	0.85 ± 0.23	1064 ± 711	20.6106 ± 0.0851	− 0.299 ± 0.107	51.212 ± 0.096	15.681	DA
15_2	266807242	34					1.3651 ± 0.1253	5.159 ± 0.164	− 8.974 ± 0.154	17.051	CV
15_2	474703167	43					1.3651 ± 0.1253	5.159 ± 0.164	− 8.974 ± 0.154	17.051	CV

[a] Group ID. i.e. '1_2" means group 1 has 2 spectra.
[b] Unique ID for each spectrum.
[c] S/N in g band. Note only spectra with S/N> = 15 in g band are fitted.
[d] Parallax from *Gaia* DR2 in mas.
[e] Proper motions in RA and Dec. from Gaia DR2 in units of mas/yr.
[f] G band photometry from Gaia DR2.

Table 5. Mis-classified WDs in LAMOST DR2. Only part of the catalogue is shown here. The full table can be found in the supplementary material.

GID[a]	RA	Dec.	Designation[b]	Mjd-Planid_spid-Fiberid[c]	snrg	Old type	Update
64_2	98.8159	2.39865	J063515.81 + 022355.1	55976-GAC_099N04_V1_sp02-124	11.73	DA_in_nebula?	star
64_2	98.8159	2.39865	J063515.81 + 022355.1	55976-GAC_099N04_V5_sp02-124	10.78	DA_in_nebula?	star
111_3	106.68858	22.26037	J070645.25 + 221537.3	56611-GAC108N21V3_sp14-199	28.55	DA + M?	star
111_3	106.68858	22.26037	J070645.25 + 221537.3	56621-GAC108N21V1_sp14-199	11.85	DA + M?	star
111_3	106.68858	22.26037	J070645.25 + 221537.3	56621-GAC108N21V3_sp14-199	15.67	DA + M?	star
113_2	58.28319	34.53968	J035307.96 + 343222.8	56618-VB057N34V1_sp08-238	17.45	DAZ	star
113_2	58.28319	34.53968	J035307.96 + 343222.8	56618-VB057N34V2_sp08-238	10.69	DAZ	star
141_1	80.71046	29.65543	J052250.50 + 293919.5	55859-M5904_sp15-198	3.41	DA?	star
142_1	10.58862	39.37988	J004221.26 + 392247.5	55862-M6201_sp16-091	5.67	DA?	star
143_1	12.11577	39.62563	J004827.78 + 393732.2	55862-M6201_sp16-122	5.27	DA?	star
151_1	89.49879	29.20391	J055759.71 + 291214.0	55876-GAC_089N28_B2_sp04-060	5.97	DA?	star
152_1	89.49431	29.98647	J055758.63 + 295911.2	55876-GAC_089N28_B2_sp15-134	3.53	DA?	star
153_1	91.57595	28.03239	J060618.22 + 280156.5	55876-GAC_089N28_B3_sp06-113	4.95	DA?	star
154_1	89.50101	29.54909	J055800.24 + 293256.7	55876-GAC_089N28_B3_sp15-102	7.67	DA?	star
156_1	88.77986	29.0578	J055507.16 + 290328.0	55876-GAC_089N28_B1_sp04-001	5.23	DA?	star
158_1	53.9205	4.24866	J033540.91 + 041455.1	55886-F8606_sp05-206	5.68	DA?	star
170_1	71.51261	26.14234	J044603.02 + 260832.4	55890-GAC_067N28_M1_sp01-236	5.18	DA?	star
171_1	74.26587	27.71918	J045703.80 + 274309.0	55890-GAC_067N28_M1_sp06-197	6.43	DA?	star
173_1	106.81713	26.6493	J070716.11 + 263857.4	55890-GAC_106N28_M1_sp01-154	9.85	DA + M?	DA
182_1	50.2794	4.86407	J032107.05 + 045150.6	55892-F9204_sp04-169	8.39	DBA?	hotSD

[a] Group ID. i.e. '1_2" means group 1 has 2 spectra.
[b] Designation from LAMOST. The exact number could be slight different for the same group.
[c] Unique spectrum ID.

Table 6. DA WDs with updated parameters in LAMOST DR2. Only part of the catalogue is shown here. The full table can be found in the supplementary material.

ObsID[a]	Designation[b]	Obsdate	RA	Dec.	snrg	Teff[c]	logg[c]	mass[c]	age[c]
112211	J221640.39 + 012741.2	2011-10-24	334.168324	1.461445	10.49	10872 ± 360	8.28 ± 0.36	0.78 ± 0.23	740 ± 400
116148	J220522.86 + 021837.5	2011-10-24	331.345250	2.310432	14.26	13000 ± 2793	7.76 ± 0.35	0.48 ± 0.16	218 ± 167
403199	J004128.66 + 402324.0	2011-10-24	10.369458	40.390026	19.99	27493 ± 2182	7.60 ± 0.35	0.46 ± 0.13	11 ± 3
1102134	J025737.24 + 264047.8	2011-10-27	44.405201	26.679970	15.86	10838 ± 359	8.51 ± 0.33	0.93 ± 0.21	1134 ± 1078
1115183	J030214.72 + 285707.4	2011-10-27	45.561340	28.952057	13.54	16814 ± 1427	7.53 ± 0.31	0.39 ± 0.10	66 ± 23
1506145	J071004.83 + 292402.8	2011-10-28	107.520140	29.400780	12.06	12000 ± 3141	6.88 ± 0.50	0.21 ± 0.10	113 ± 147
1615243	J004036.79 + 413138.7	2011-10-28	10.153296	41.527443	21.71	13564 ± 2707	7.83 ± 0.32	0.52 ± 0.17	209 ± 183
1616129	J003956.55 + 422929.5	2011-10-28	9.985629	42.491542	10.24	9861 ± 303	7.76 ± 0.55	0.47 ± 0.26	472 ± 266
2101118	J005340.52 + 360116.8	2011-11-08	13.418857	36.021358	32.82	28460 ± 1577	7.85 ± 0.33	0.57 ± 0.15	10 ± 1
2102081	J004159.19 + 362352.3	2011-11-08	10.496630	36.397865	10.03	22062 ± 2314	7.60 ± 0.33	0.44 ± 0.13	24 ± 9
6610008	J032942.79 + 053755.8	2011-11-20	52.428301	5.632185	11.08	19155 ± 1518	8.04 ± 0.27	0.65 ± 0.16	91 ± 67
6807221	J063532.48 + 261958.6	2011-11-20	98.885366	26.332951	14.00	35843 ± 2393	8.00 ± 0.42	0.67 ± 0.21	5 ± 2
6904155	J080800.00 + 290152.5	2011-11-20	122.000010	29.031273	19.48	25340 ± 2300	7.93 ± 0.32	0.60 ± 0.15	17 ± 8
7015243	J004036.79 + 413138.7	2011-11-20	10.153296	41.527443	19.41	13000 ± 2414	7.86 ± 0.35	0.53 ± 0.19	249 ± 201
7516178	J071004.83 + 292402.8	2011-11-23	107.520140	29.400789	12.04	13758 ± 1742	8.16 ± 0.30	0.71 ± 0.19	324 ± 226
7801231	J100551.51-023417.8	2011-11-24	151.464628	−2.571630	19.69	20835 ± 1816	7.99 ± 0.30	0.62 ± 0.17	55 ± 58

Notes.[a] Unique ID for each spectrum.
[b] Designation from LAMOST. The exact number could be slight different for the same group.
[c] Undated parameters using fitting method adopted in this work.

5 SUMMARY

In this work, we study the DAs and DBs identified in LAMOST DR5. The LAMOST pipeline classification, colour-colour cut, and RF method were utilized to select DA candidates. Visual inspection produced 2620 authentic DA spectra. For DBs, a RF, machine learning algorithm was used to select the candidates. From 12 572 DB candidates, 182 were visually confirmed. Regarding the efficiency, larger training sample in the future can definitely be helpful. After cross-matching with SIMBAD and the literature, 393 DAs and 46 DBs are found to be new identifications.

Those identified WDs were analysed. For all DAs, where their spectral S/N >10, and DBs with same S/N >10, their spectra were fitted with WD atmosphere models to derive effective temperature and surface gravity (Koester 2010). From these two parameters, the mass and cooling age were calculated from evolutionary models.

Proper motions, magnitude, and parallax of *Gaia* DR2 are also provided in our catalogue (Table 4). In addition, distributions of mass, effective temperature, surface gravity, cooling age, and distance were built to study the property of our sample.

For DAs, the peak of the mass distribution is in general agreement with previous results. Both low- and high-mass residuals are present in the mass distributions. For DBs, the peak of the mass distribution is located around 0.65 $M_{\odot}$, and also consistent with other studies. However, there are only 70 DBs with sufficiently high S/N to derive reliable parameters, and the resulting distributions are too sparsely populated to draw any conclusions. The parameters of LAMOST DAs and DBs have been compared for sources in common with previous work, and found to be in good agreement for spectra with relatively high S/N. We also found that for spectra with LAMOST S/N less than ∼50, SDSS spectra tend to have larger S/N, whilst for spectra with S/N greater than ∼50, LAMOST spectra have larger S/N.

Even after the release of *Gaia* DR2 (Gaia Collaboration 2018a) and the WD candidates catalogue in *Gaia* (Gentile Fusillo et al. 2018), the observation of optical WD spectra is still of great importance.

Optical spectral identification is of increasing importance in the *Gaia* era. Therefore, we selected 20 628 WD candidates from XSTPS-GAC and GPS1, then put them into the input catalogue of low-resolution observation for the transition year and second phase of LAMOST, which began in 2017. Since the WD candidates catalogue from *Gaia* DR2 has been published, we will try to add those observable candidates into LAMOST inout catalogue in the near future as well.

ACKNOWLEDGEMENTS

We thank the anonymous referee for helpful suggestions and advices, which improved this paper a lot. We thank M. Barlow, J. Farihi, and A. Swan for a careful reading of the manuscript and helping with the improvement of English writing. We also thank D. Koester and P. Bergeron for providing WD models. Balmer/Lyman lines in the models were calculated with the modified Stark broadening profiles of Tremblay & Bergeron (2009), kindly made available by the authors. This work is supported by the National Natural Science Foundation of China (grant no. 11890694, 11473001, and 11078006). The authors also acknowledge support by the National Key Basic Research Program of China (grant no. 2014CB845700). We also acknowledge the support from the 2m Chinese Space Station Telescope project: CMS-CSST-2021-A10. This work is partially supported by the Scholar Program of Beijing Academy of Science and Technology (DZ: BS202002). This work is also supported by the China Postdoctoral Science Foundation (grant no. 2017M610695) and the Astronomical Big Data Joint Research Centre, co-founded by the National Astronomical Observatories, Chinese Academy of Sciences, and the Alibaba Cloud.

The LAMOST FELLOWSHIP is supported by Special Funding for Advanced Users, budgeted, and administrated by the Centre for Astronomical Mega-Science, Chinese Academy of Sciences.

The Guo Shou Jing Telescope (the Large Sky Area Multi-Object Fibre Spectroscopic Telescope, LAMOST) is a National Major Scientific Project which is built by the Chinese Academy of Sciences, funded by the National Development and Reform Commission, and operated and managed by the National Astronomical Observatories, Chinese Academy of Sciences.

This research has made use of the SIMBAD data base, operated at CDS, Strasbourg, France. This work has used the software ASERA for visual inspection. Many thanks to the author Yuan et al. (2013).

DATA AVAILABILITY

The spectra data underlying this article are publicly available from LAMOST archive (http://dr5.lamost.org/). Tables 3–6 are partially

shown in the article. They are fully accessible through publisher in supplementary material. Tables 5 and 6 are WDs identified in our previous work (LAMOST DR2) with updated classifications and parameters.

REFERENCES

Abazajian K. N. et al., 2009, ApJS, 182, 543
Ahn C. P. et al., 2014, ApJS, 211, 17
Bai Y., Liu J.-F., Wang S., 2018, RAA, 18, 118
Bai Y., Liu J., Wang S., Yang F., 2019, AJ, 157, 9
Bergeron P., Leggett S. K., Ruiz M. T., 2001, ApJS, 133, 413
Bovy J., 2017, MNRAS, 468, L63
Breiman. L., 2001, Mach. Learn., 45, 5
Carlin J. L. et al., 2012, Res. Astron. Astrophys., 12, 755
Catalán S., Isern J., García-Berro E., Ribas I., 2008a, MNRAS, 387, 1693
Catalán S., Isern J., García-Berro E., Ribas I., Allende Prieto C., Bonanos A. Z., 2008b, A&A, 477, 213
Chen L. et al., 2012, Res. Astron. Astrophys., 12, 805
Cui X.-Q. et al., 2012, Res. Astron. Astrophys., 12, 1197
Cunningham T., Tremblay P.-E., Gentile Fusillo N. P., Hollands M., Cukanovaite E., 2020, MNRAS, 492, 3540.
Dalton G. et al., 2012, Proc. SPIE, 8446, 84460P
de Jong R. S. et al., 2012, Proc. SPIE, 8446, 84460T
Deng L.-C. et al., 2012, Res. Astron. Astrophys., 12, 735
DESI Collaboration, Aghamousa A., Aguilar J., Ahlen S., Alam S., Allen L. E., Allende Prieto C., et al., 2016, arXiv (arXiv:1611.00036)
Doherty C. L., Gil-Pons P., Siess L., Lattanzio J. C., Lau H. H. B., 2015, MNRAS, 446, 2599.
Du B. et al., 2016, ApJS, 227, 27
Eisenstein D. J. et al., 2006, ApJS, 167, 40
Farihi J., Gänsicke B. T., Koester D., 2013, Science, 342, 218
Fontaine G., Brassard P., Bergeron P., 2001, PASP, 113, 409
Gaia Collaboration, 2016, A&A, 595, A1
Gaia Collaboration, 2018a, A&A, 616, A1
Gaia Collaboration, 2018b, A&A, 616, A11
Gänsicke B. T., Koester D., Farihi J., Girven J., Parsons S. G., Breedt E., 2012, MNRAS, 424, 333
Gänsicke B. T., Marsh T. R., Southworth J., Rebassa-Mansergas A., 2006, Science, 314, 1908
Gentile Fusillo N. P. et al., 2015, MNRAS, 452, 765
Gentile Fusillo N. P. et al., 2019, MNRAS, 482, 4570
Gentile Fusillo N. P., Tremblay P.-E., Jordan S., Gänsicke B. T., Kalirai J. S., Cummings J., 2018, MNRAS, 473, 3693
Girven J., Gänsicke B. T., Steeghs D., Koester D., 2011, MNRAS, 417, 1210

Green R. F., Schmidt M., Liebert J., 1986, ApJS, 61, 305
Guo J.-C. et al., 2018, Res. Astron. Astrophys., 18, 32
Guo J.-C. et al., 2019, Res. Astron. Astrophys., 19, 008
Guo J.-C., Liu C., Liu J.-F., 2016, Res. Astron. Astrophys., 16, 44
Guo J., Tziamtzis A., Wang Z., Liu J., Zhao J., Wang S., 2015a, ApJ, 810, L17
Guo J., Zhao J., Tziamtzis A., Liu J., Li L., Zhang Y., Hou Y., Wang Y., 2015b, MNRAS, 454, 2787
Harris H. C. et al., 2006, AJ, 131, 571
Heger A., Fryer C. L., Woosley S. E., Langer N., Hartmann D. H., 2003, ApJ, 591, 288
Holberg J. B., Oswalt T. D., Sion E. M., McCook G. P., 2016, MNRAS, 462, 2295
Hollands M. A., Tremblay P.-E., Gänsicke B. T., Gentile-Fusillo N. P., Toonen S., 2018, MNRAS, 480, 3942
Jiang B., Luo A., Zhao Y., Wei P., 2013, MNRAS, 430, 986
Jiménez-Esteban F. M., Torres S., Rebassa-Mansergas A., Skorobogatov G., Solano E., Cantero C., Rodrigo C., 2018, MNRAS, 480, 4505
Kaiser N. et al., 2010, Proc. SPIE, 7733, 77330E
Kalirai J. S., Hansen B. M. S., Kelson D. D., Reitzel D. B., Rich R. M., Richer H. B., 2008, ApJ, 676, 594
Kalirai J. S., Saul Davis D., Richer H. B., Bergeron P., Catelan M., Hansen B. M. S., Rich R. M., 2009, ApJ, 705, 408
Kepler S. O. et al., 2015, MNRAS, 446, 4078
Kepler S. O. et al., 2016, MNRAS, 455, 3413
Kepler S. O. et al., 2019, MNRAS, 486, 2169
Kepler S. O., Kleinman S. J., Nitta A., Koester D., Castanheira B. G., Giovannini O., Costa A. F. M., Althaus L., 2007, MNRAS, 375, 1315
Kilic M., Bergeron P., Dame K., Hambly N. C., Rowell N., Crawford C. L., 2019, MNRAS, 482, 965
Kilic M., Hambly N. C., Bergeron P., Genest-Beaulieu C., Rowell N., 2018, MNRAS, 479, L113
Kilic M., Munn J. A., Harris H. C., von Hippel T., Liebert J. W., Williams K. A., Jeffery E., DeGennaro S., 2017, ApJ, 837, 162
Kleinman S. J. et al., 2004, ApJ, 607, 426
Kleinman S. J. et al., 2013, ApJS, 204, 5
Koester D., 2010, Mem. Soc. Astron. Ital., 81, 921
Koester D., Kepler S. O., 2015, A&A, 583, A86
Kollmeier J. A., Zasowski G., Rix H.-W., Johns M., Anderson S. F., Drory N., Johnson J. A., 2017, arXiv (arXiv:1711.03234)
Kong X., Luo A.-L., 2019, ASP Conf. Ser., 523, 91
Krzesinski J., Kleinman S. J., Nitta A., Hügelmeyer S., Dreizler S., Liebert J., Harris H., 2009, A&A, 508, 339
Lam M. C. et al., 2019, MNRAS, 482, 715
Li Y.-B. et al., 2018, ApJS, 234, 31
Liebert J., Bergeron P., Holberg J. B., 2005, ApJS, 156, 47
Liu C. et al., 2014, ApJ, 790, 110
Luo A.-L. et al., 2015, Res. Astron. Astrophys., 15, 1095
Manser C. J. et al., 2019, Sci, 364, 66
Markwardt C. B., 2009, ASP Conf. Ser., 411, 251
McCook G. P., Sion E. M., 1987, ApJS, 65, 603
McCook G. P., Sion E. M., 1999, ApJS, 121, 1
Melis C., Dufour P., Farihi J., Bochanski J., Burgasser A. J., Parsons S. G., G"ansicke B. T., 2012, ApJ, 751, L4
Munn J. A., Harris H. C., von Hippel T., Kilic M., Liebert J. W., Williams K. A., DeGennaro S., 2017, AJ, 153, 10
Pedregosa F. et al., 2011, J. Mach. Learn. Res., 12, 2825
Rebassa-Mansergas A. et al., 2015, MNRAS, 450, 743
Ren J.-J., Rebassa-Mansergas A., Parsons S. G., Liu X.-W., Luo A.-L., Kong X., Zhang H.-T., 2018, MNRAS, 477, 4641
Rolland B., Bergeron P., Fontaine G., 2018, ApJ, 857, 56
Rowell N., 2013, MNRAS, 434, 1549
Rowell N., Kilic M., 2019, MNRAS, 484, 3544
Tian H.-J. et al., 2017, ApJS, 232, 4
Torres S., Cantero C., Rebassa-Mansergas A., Skorobogatov G., Jiménez-Esteban F. M., Solano E., 2019, MNRAS, 485, 5573
Tremblay P.-E. et al., 2020, MNRAS, 497, 130
Tremblay P.-E., Bergeron P., 2009, ApJ, 696, 1755
Tremblay P.-E., Bergeron P., Gianninas A., 2011, ApJ, 730, 128
Wei P. et al., 2014, AJ, 147, 101
Wood M. A., 1990, PhD Thesis, Univ. Texas
Wood M. A., 1995, Lecture Notes Phys., 443, 41
York D. G. et al., 2000, AJ, 120, 1579
Yuan H.-B. et al., 2015, MNRAS, 448, 855
Yuan H., Zhang H.,, Zhang Y., Lei Y., Dong Y., Zhao Y., 2013, A&C, 3, 65
Zhang Y.-Y. et al., 2013, AJ, 146, 34
Zhao G., Zhao Y.-H., Chu Y.-Q., Jing Y.-P., Deng L.-C., 2012a, Res. Astron. Astrophys., 12, 723
Zhao J. K., Luo A. L., Oswalt T. D., Zhao G., 2013, AJ, 145, 169
Zhao J. K., Oswalt T. D., Willson L. A., Wang Q., Zhao G., 2012b, ApJ, 746, 144

SUPPORTING INFORMATION

Supplementary data are available at *MNRAS* online.

Table3.dat
Table4.dat

Table5.dat
Table6.dat
Table 3. Basic parameters of WDs from LAMOST DR 3, 4, and 5.
Table 4. Determined WD parameters and parameters from Gaia DR2.
Table 5. Mis-classified WDs in LAMOST DR2.
Table 6. DA WDs with updated parameters in LAMOST DR2.

This paper has been typeset from a TEX/LATEX file prepared by the author.